Quarterly Journal of the
Royal Meteorological Society

Ocean Ensemble Forecasting, Part II: Mediterranean Forecast System Response

Journal:	*QJRMS*
Manuscript ID:	QJ-09-0239
Wiley - Manuscript type:	Research Article
Date Submitted by the Author:	13-Nov-2009
Complete List of Authors:	Bonazzi, Alessandro; INGV, Operational Oceanography Group Pinardi, Nadia; University of Bologna, CIRSA Dobricic, Srdjan; CMCC Milliff, Ralph; NorthWest Research Associates, Colorado Research Associates Division Wikle, Christopher; University of Missouri, Statistics Berliner, L.; Ohio State University, Statistics
Keywords:	Ocean Ensemble Forecasting, Ensemble Perturbations, Forecast Spread

Ocean Ensemble Forecasting, Part II: Mediterranean Forecast System Response

Alessandro Bonazzi

Operational Oceanography Group, INGV; Bologna, ITALY

Nadia Pinardi

CIRSA, University of Bologna, Ravenna, ITALY

Srdjan Dobricic

Centro EuroMediterraneo per i Cambiamenti Climatici, Bologna, ITALY

Ralph F. Milliff

NWRA, Colorado Research Associates Div.; Boulder, CO, USA

Christopher K. Wikle

Statistics Department, University of Missouri; Columbia, MO, USA

L. Mark Berliner

Statistics Department, Ohio State University; Columbus, OH, USA

14 November 2009

ABSTRACT

This paper analyzes the ocean forecast response to surface vector wind (SVW) distributions generated by a Bayesian Hierarchical Model (BHM) developed in Part I (Milliff et al., 2009). A new method for Ocean Ensemble Forecasting (OEF), so-called BHM-SVW-OEF, is described. BHM-SVW realizations are used to produce and force perturbations in the ocean state during 14-day analysis and 10-day forecast cycles of the Mediterranean Forecast System (MFS). The BHM-SVW-OEF ocean response spread is amplified at the mesoscales and pycnocline of the eddy field. The new method is compared to an ensemble response forced by ECMWF Ensemble Prediction System (EEPS) surface winds, and to an ensemble forecast started from perturbed initial conditions derived from an *ad hoc* Thermocline Intensified Random Perturbation (TIRP) method. The EEPS-OEF shows spread at the basin scales while the TIRP-OEF response is mesoscale intensified as in the BHM-SVW-OEF response. TIRP-OEF perturbations fill more of the MFS domain while the BHM-SVW-OEF perturbations are more location-specific, concentrating ensemble spread at the sites where the ocean model response to uncertainty in the surface wind forcing is largest. The BHM-SVW-OEF method offers a practical and objective means for producing short-term forecast spread by modeling surface atmospheric forcing uncertainties that have maximum impact at the ocean mesoscales.

1 Introduction

The aims of this paper are: 1) to analyze the impact of the Bayesian Hierarchical Model (BHM) Surface Vector Winds (SVW) derived in Part I (BHM-SVW, Milliff et al., 2009) on the Ocean Ensemble Forecast (OEF) response; and 2) to compare the response with other ensemble forecast generating methods. The assessment will be carried out for the short-term, open-ocean Mediterranean Forecasting System (MFS, Pinardi et al., 2003 and 2009). The MFS produces deterministic ten-day ocean forecasts starting from ocean analyses that incorporate both satellite and *in situ* data. The MFS ocean forecasting model is eddy resolving and mesoscale variability dominates the flow field on weekly timescales. Phase and amplitude errors associated with the eddies are the main causes of forecast predictability loss and forecast errors in temperature, salinity and sea level double on time scales of a few days (Tonani et al., 2009).

Given that the predictability limit of short term ocean forecasting is associated with the oceanic mesoscale eddies, any ocean ensemble forecasting method should consider both initial condition and atmospheric forcing errors. Starting from uncertainty in the atmospheric SVW fields, Part I of this paper constructed an ensemble of initial conditions consistent with the assimilation of observations and atmospheric wind errors during the analysis cycle of MFS. This paper will now study the characteristics of the 10-day OEF standard deviation, i.e. the spread, deriving from the ensemble initial conditions and the BHM-SVW forecast wind realizations.

The BHM-SVW-OEF spread will be compared to the ensemble standard deviation produced with: 1) wind realizations coming from the European Centre for Medium Range Weather Forecast (ECMWF) Ensemble Prediction System (EPS); and 2) a fixed initial condition perturbation method, already shown to be efficient for producing spread at ocean mesoscales (Pinardi et al., 2008). The sensitivity of the OEF spread to the ocean forecast model horizontal resolution will also be studied for both the BHM-SVW and ECMWF EPS ensemble generating methods.

The impact of wind forcing errors on ocean ensemble forecasts has been studied by other authors. Burillo et al. (2002) develope a pseudo-random perturbation method for the winds and perform 100 forecasts with the same initial condition, generating ensemble spread in the mixed layer (first 100 meters). Auclair et al. (2003) uses again pseudo-random perturbations of the winds, initial density, the lateral boundary conditions and the river inputs, for a

coastal model domain. They show that the model response spread is sensitive to each perturbation type depending on the dominant ocean current regime. Lucas et al. (2008) perturb winds, air temperature and incoming solar radiation fields deducing the errors from the comparison of the ECWMF re-analyses forcing fields with data from the Co-ordinated Ocean-Ice Reference Experiments (CORE). Again, the perturbations to the ECMWF re-analysis fields are modeled in a pseudo-random way and the ocean response peaks in the eddy field of the Gulf Stream and tropical regions of the North Atlantic. However, the perturbations at 100 meters need several months to grow, limiting the utility for real-time daily ensemble forecasting systems. These previous attempts did not use realistic estimates of the atmospheric wind errors as we have developed with the BHM-SVW method, and they did not use model adjusted initial condition perturbations, as we have shown in Part I of this paper (Milliff et al., 2009).

In section 2 we describe the main characteristics of the MFS operational ocean forecasting system and the different resolution models used in this paper. Section 3 describes the two ensemble generating methods from BHM and ECMWF EPS winds and section 4 offers the comparison of ensemble responses to the two methods. Section 5 describes an alternative initial condition perturbation method and the comparison with the previous ensemble results. Section 6 describes the vertical temperature and salinity structure of the ensemble variance generated by the BHM-SVW-OEF method and section 7 provides a summary and conclusions.

2 The Mediterranean Forecasting System: assimilation scheme and models

The MFS[1] is composed of a large observational network, a numerical prediction model and a data assimilation scheme. The observational network consists of real time satellite and in situ data. The latter includes temperature vertical profiles down to 700 meters provided by a ship of opportunity program (Manzella et al., 2007), and temperature and salinity profiles down to 700 and 2000 meters implemented by the MedArgo program (Poulain at al. 2007). The real-time satellite measurements include along track Sea Level Anomaly (SLA) from altimetry (Le Traon et al. 2003) and Sea Surface Temperature (SST; Buongiorno Nardelli

[1]http://gnoo.bo.ingv.it/mfs

et al., 2003).

The MFS ocean model is described in Tonani et al. (2008) and here we outline only its main characteristics. The model has 71 non-uniform z-coordinates levels and a horizontal resolution of $1/16^\circ \times 1/16^\circ$. The model domain covers the Mediterranean Sea and a portion of the Atlantic Ocean where an Atlantic box is designed to parameterize coupling between the Mediterranean and the Atlantic. The operational model is forced by ECMWF surface fields using interactive air-sea physics (Tonani et al., 2008, Pettenuzzo et al., 2009). A lower resolution implementation of the MFS numerical ocean model, with 71 vertical levels and a horizontal resolution of $1/4^\circ \times 1/4^\circ$ is also used in this paper. The geographical domain of the low-resolution model is the same as the high-resolution model except for the Atlantic box which is taken from previous investigations at the lower resolution (Korres et al., 2000, Brankart and Pinardi, 2002). In the following, the high- and low-resolution versions of the MFS models are referred to as MFS1671 and MFS471 respectively. The MFS471 model is initialized from MFS1671 fields using bilinear interpolation.

The atmospheric forcing used in MFS is derived from the ECMWF analysis fields and the 10 day ECMWF single deterministic forecast fields, starting at 12:00 UTC. The ECMWF forecast model has a spectral representation with a triangular truncation of 511 waves in the horizontal and 60 levels in the vertical (T511L60) which means a nominal horizontal resolution of $40\,km$. The surface fields are utilized in a reduced regular grid of 0.5 x 0.5 degrees of latitude and longitude. The ECMWF surface fields, i.e. SVW, mean sea level pressure, air temperature, relative humidity are used in bulk formulas (Pettenuzzo et al., 2009) that, combined with the model SST, provide momentum and heat fluxes to the ocean model. The ocean operational forecast outputs that use the deterministic ECMWF SVW forecast fields will be called hereafter control forecasts.

All the real time data are assimilated in both ocean models using a reduced order optimal interpolation scheme adapted by Dobricic et al. (2007) to produce daily ocean analyses. Ocean state analyses are constructed using ECMWF surface analysis forcing fields and by assimilating available ocean data using a one day temporal window. In Figure 1, the MFS analysis and control forecast cycle is schematized. At day J of the week, a 14-day analysis period is started from day J-14 to J-1 producing 1A to 14A analysis fields. A control forecast is then started from the 14A analysis snapshot (Day 0 of the forecast period), producing 1F to 10F control forecast fields. Both the MFS1671 and MFS471 models use the same

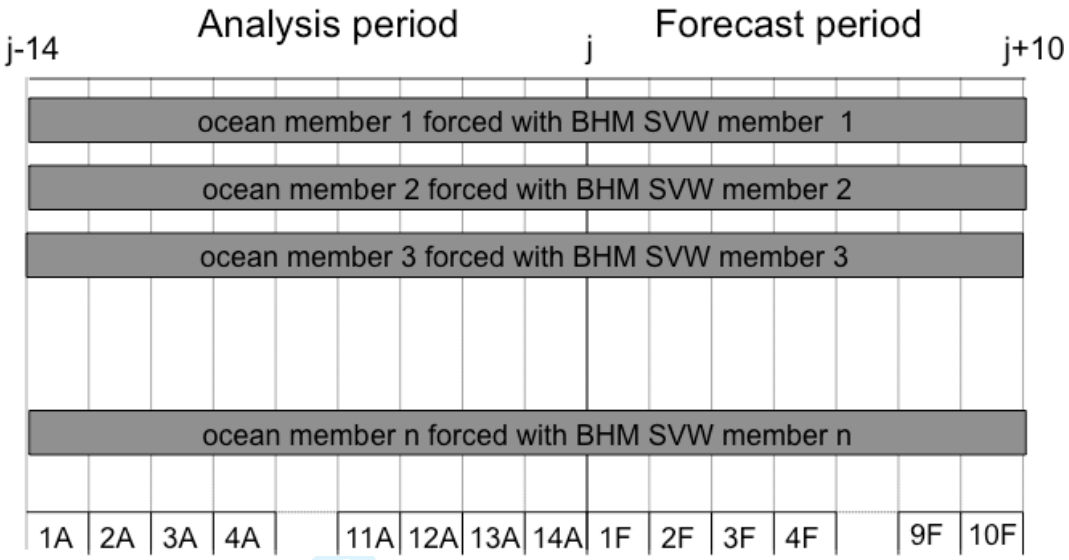

Figure 1: Schematic of the MFS analysis and control forecast cycle and the BHM-SVW-OEF method: J indicates the day at which the forecasts start, the 1A to 14A and 1F to 10F symbols indicate analysis and forecast days respectively. The BHM-SVW members are used to force n OEF members starting from perturbed initial conditions at day J.

assimilation scheme, observational data and deterministic atmospheric forcings.

3 Ocean Ensemble Methods generated by wind ensembles

In the following two subsections we will describe the two ocean ensemble forecast methods that use wind forcing perturbations to generate ocean ensemble forecasts.

3.1 The BHM-SVW Ocean Ensemble Forecast method

The BHM-SVW posterior distributions, developed in Part I of this paper (Milliff et al., 2009) are used to design a new ensemble forecast method, so-called BHM-SVW Ocean Ensemble Forecast (OEF) method. The method samples realizations of SVW produced by the BHM to force the ocean models during the ocean analysis period, leading to an ensemble of ocean initial conditions from which ensemble ocean forecasts can be started. The differences with

respect to other existing methods are twofold: 1) the wind realizations force the models during the assimilation cycle in order to produce initial condition perturbations; and 2) the BHM-SVW realizations transition smoothly between the analysis and forecast periods. The first difference insures that perturbations grow in the ocean field only where observations are not sufficient to reduce the initial condition uncertainty. The second difference insures that the ensemble forecast and analysis wind fields have distribution variances that are smoothly changing across the analysis and forecast periods.

The BHM-SVW-OEF method is then designed as follows (Fig. 1). During the 14-day analysis period, each ocean ensemble member is forced with a different BHM-SVW realization, while assimilating the ocean temperature, salinity and SLA observations. The n ocean initial conditions produced at day J are then forced with the corresponding n BHM SVW realizations in the forecast period. The BHM-SVW data stage contains QuickSCAT data and ECMWF analyses during the 1A-14A period and the ECWMF deterministic forecast during the 1F-10F period. The BHM-SVW process model used in this work is the A1E3 version of the Rayleigh friction equation model described in Part I of this paper (Milliff et al., 2009). The number of ensemble members is 10 for MFS1671 and 100 for MFS471. It is important to note that the BHM-SVW realizations produce not only perturbed wind stresses and thus momentum fluxes, but also perturbed surface heat and water fluxes as well. Using interactive bulk formulae in the model together with BHM-SVW perturbs all surface fluxes affected by uncertainty in surface winds.

3.2 The EEPS-Ocean Ensemble Forecast method

The second ocean ensemble forecast method studied in this paper uses SVW realizations from the ECMWF Ensemble Prediction System (EEPS). We call this method the EEPS Ocean Ensemble Forecast (EEPS-OEF). EEPS for the global atmosphere has proven to be useful in a wide range of applications (Buizza, 2006). However, the utility of EEPS surface winds as forcing to generate ocean ensemble forecasts has not been tested. It will be compared here with the BHM-SVW-OEF method.

EEPS uses singular vectors to perturb the atmospheric forecast initial conditions (Lacarra and Talagrand, 1988; Farrell, 1990). The singular vectors identify patterns with maximum growth rates within the first 48 hrs of the forecast and for the synoptic scales. Small errors in the initial condition state will amplify most rapidly in patterns corresponding to the leading

singular vectors, and will affect the forecast accuracy (Buizza, 1995). Since the end of 2000 and up to 2005, the operational implementation of the EEPS includes 50 perturbed members at T255L62 resolution, plus an unperturbed forecast (i.e. 51 ensemble members in total). The nominal resolution of the EEPS winds is approximately 80 km, i.e. two times lower than the deterministic ECMWF forecast winds.

The EEPS-OEF method makes use of a single analysis field snapshot at 14A as the initial condition for the ocean forecast. For the high-resolution model, MFS1671, 10 forecasts are forced by EEPS wind members. For the low-resolution model, MFS471, all 51 members of the EEPS are used. The EEPS-OEF method has a clear disadvantage in terms of producing useful spread in the ensemble forecast since it starts from an unperturbed initial condition.

Figure 2 shows the posterior SVW amplitude standard deviation generated by the BHM, by EEPS, and the comparison with the root mean square (rms) forecast error. The latter is defined as the rms of the difference between ECMWF 10-day deterministic wind forecasts and the corresponding wind analyses, computed for 255 10-day forecast periods in the years 2000-2004, and averaged over the basin. The BHM-SVW and the EEPS wind spread are instead calculated for the period from 25 January to 17 February 2005 only. For EEPS the spread is calculated as the standard deviation from the mean of the 51 ensemble members. The BHM-SVW amplitude, $W(x, y, t) = |\vec{U}|$, is calculated from the $\vec{U}$ BHM realizations and the distribution is given by:

$$W(x, y, t) \sim N(W_{mean}(x, y, t), \sigma_W^2) \tag{1}$$

(for notation see Part I, Milliff et al., 2009) where x, y, t denote space and time coordinates and σ_W is the standard deviation represented in Figure 2.

Clearly, different concepts of uncertainty are being implemented in the EEPS and BHM SVW distributions. For the BHM-SVW case, the uncertainties in the surface wind during the analysis period derive from parameters selected to represent observational errors (i.e. for QuikSCAT and ECMWF analysis winds) and process model errors. During the forecast period the error parameters represent uncertainties in the ECMWF forecast winds and the process model (Milliff et al., 2009). Figure 2 shows that the spread varies periodically during the period 1A-14A due to the insertion of scatteromenter data. The spread remains constant during the forecast period since the ECMWF forecast wind variance has been modeled as time independent (see Part I, Milliff et al., 2009). The EEPS wind spread (blue curve) mimics

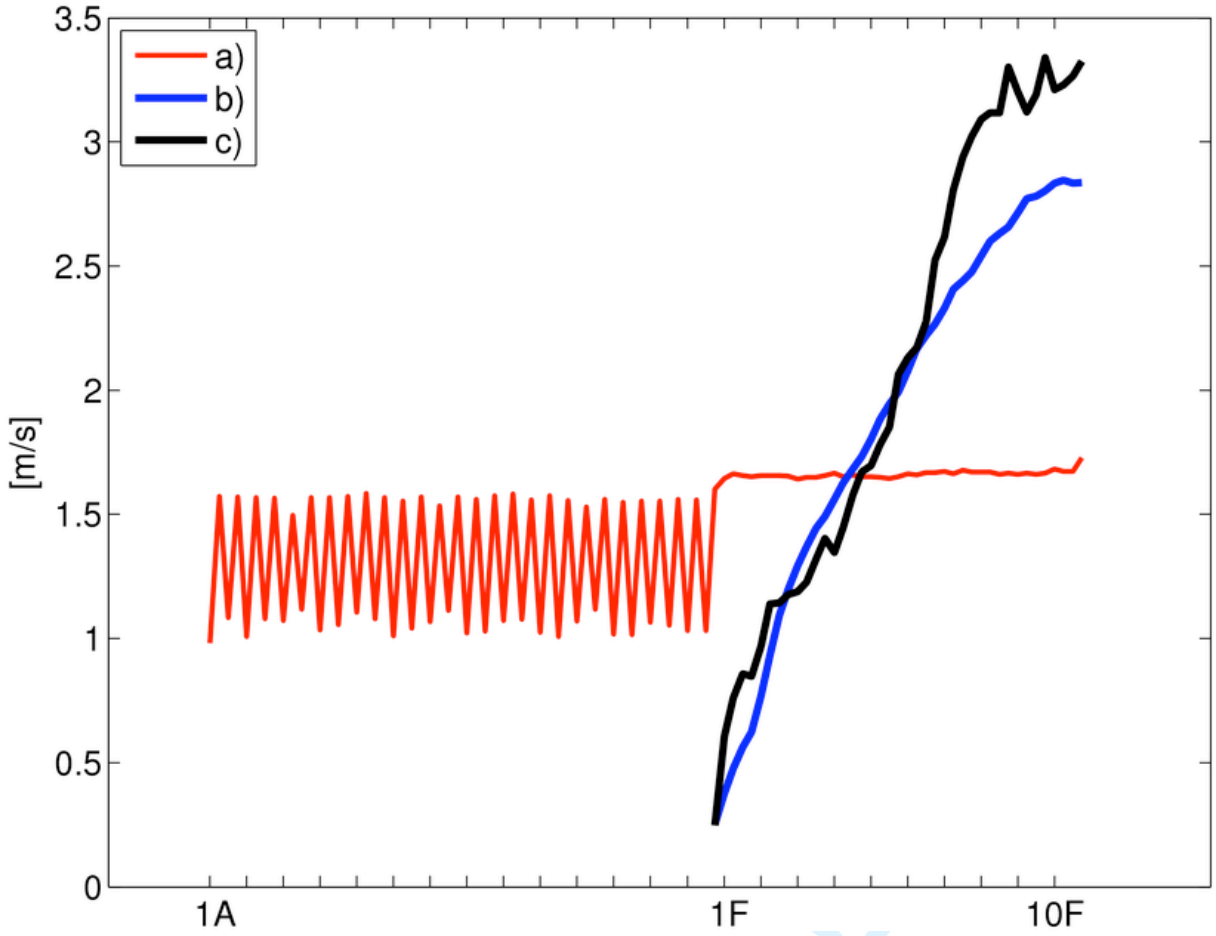

Figure 2: Comparison of wind amplitude spread for different wind ensemble generating methods and the ECMWF surface wind forecast errors. a) Wind amplitude spread σ_W (see equation 1) of BHM-SVW distribution in the analysis and forecast periods (25 January to 7 February 2005 (1A-14A), 8 to 17 February 2005 (1F-10F)). b) same as (a) but for EEPS winds during the forecast period. c) ECMWF root mean square forecast error computed for the period 2000-2004 and averaged over the basin.

instead the growth of the forecast error (black curve), albeit offset to lower amplitude after day 6F. The BHM-SVW amplitude spread during 1F-10F period is slightly larger than 1.5 ms^{-1} which is the spread of EEPS winds and the forecast error at day 5F.

It is important to note the difference between EEPS and BHM SVW distribution spread at 1F. The BHM-SVW method smoothly carries the variance information from the analysis time to the forecast period without discontinuities. EEPS instead jumps from almost zero at the forecast initial time to a value larger than 2.5 ms^{-1}. This discontinuity may cause unwanted response in the ocean forecast ensemble and contamination by ocean surface gravity waves, as has been shown in other papers (Powell et al., 2008).

In order to better describe the differences between EEPS and BHM-SVW distributions, Figure 3 shows snapshots of the SVW and wind curl from the two data sets in the northwestern Mediterranean Sea (Gulf of Lyon) during a Mistral event occurring on 14 February 2005, i.e. day 7F. Three realizations are shown from the EEPS and BHM-SVW ensemble winds. The amplitude of the wind curl is large over wider areas in the unperturbed EEPS forecast, probably due to the low resolution of the EPS atmospheric model. EEPS members differ in synoptic-scale patterns while the BHM-SVW are different at finer spatial scales; i.e. sub-synoptic or atmospheric mesoscales. The scales of uncertainty given by these two wind ensembles are not overlapping since the EEPS distributions focus on the error growth in the 500 hPa geopotential height field while the BHM-SVW focus on the surface wind errors as characterized by QuikSCAT. Our analyses indicate that the surface atmospheric flow field exhibits finer spatial scale errors probably due to orographic effects and land-sea temperature and humidity differences. In the sections below, we will show that the smaller-scale uncertainties in the wind field realizations are important in generating an ensemble response at the ocean mesoscale.

4 Comparison of BHM-SVW and EEPS Ocean Ensemble Forecast Methods

In this section we compare the ocean responses of the two ensemble ocean forecast perturbation methods described in the previous section for the high-resolution, MFS1671, and the low-resolution, MFS471, model systems. The ocean ensemble forecast initial conditions are generated by BHM-SVW-OEF in the period 25 January to 7 February 2005 (1A-14A),

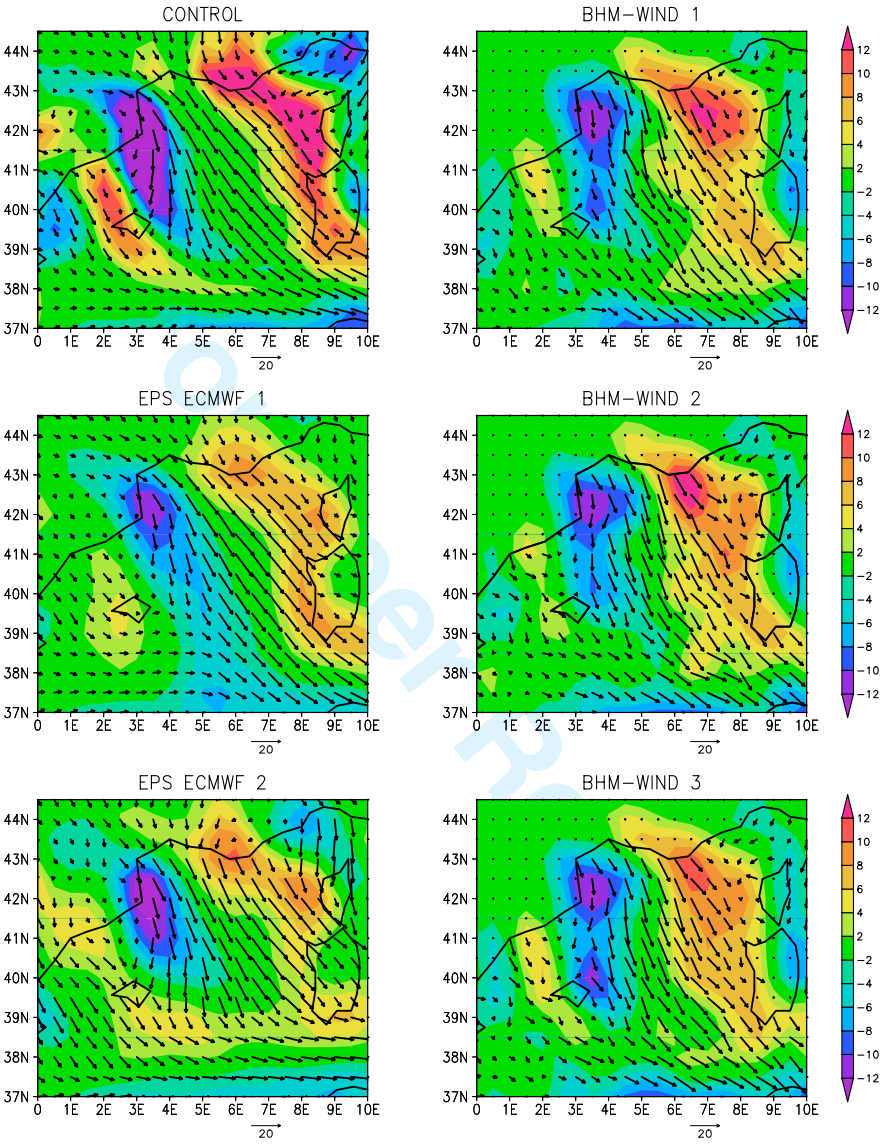

Figure 3: Western Mediterranean (Gulf of Lyon) wind fields from 3 realizations of the EEPS (left column, including the unperturbed EPS fields at the top left) and the BHM-SVW (right column). Surface winds (vectors $[m/s]$) and wind curl (color contours $[Nm^{-3} * 10^6]$) for 14 February 2005 at 00:00 UTC, day 7F.

while the forecast period is from 8 to 17 February 2005 (1F-10F). We call this the canonical ensemble forecast experiment which is carried out in parallel to the control MFS forecast.

The ocean initial condition spread for the BHM-SVW-OEF with MFS1671 has been discussed in Part I (Milliff et al., 2009). We have shown there that the initial condition spread in Sea Surface Height (SSH) and Sea Surface Temperature (SST) is located in specific regions of the basin, where we suspect ocean hydrodynamic instabilities, eddy interaction and eddy propagation processes are occurring.

4.1 High-Resolution Model Ensemble Response

Figure 4 compares the BHM-SVW-OEF and EEPS-OEF responses at the end of the forecast period (day 10F, 17 February 2005) for the MFS1671 model. The daily mean SSH for the control forecast at day 10F (Fig. 4, panel a) shows high SSH and intense gradients along the southern coastlines of the basin and along the northern Levantine coastline, off Turkey. Local maxima occur in the Algerian current ($6°E$, $38.5°N$) and in the area of the Mersa-Matruh gyre ($29°E$, $32°N$). Sub-basin scale cyclonic gyre circulations are indicated by SSH minima in the Gulf of Lyon ($5°E$, $42°N$), the central Ionian Sea ($19°E$, $38°N$) and in the Rhodes Gyre region of the Levantine Sea ($27.5°E$, $35°N$).

Fig. 4, panel b shows that the BHM-SVW-OEF spread is localized in specific regions, at the scale of the eddies, and it has doubled in amplitude from the initial condition values (see Part I, Milliff et al., 2009). The spread is associated with large gradients in the SSH field that identify currents (i.e., the Algerian current in the western basin, from $0°E$ to $10°E$, the Atlantic-Ionian Stream in the central Ionian Sea, from $15°E$ to $20°E$, and the North African current up to the western edge of the Mersa Matruh Gyre in the Levantine basin, from $20°E$ to $30°E$). In these regions SSH spread for BHM-SVW-OEF reaches values of $6\,cm$. On the other hand, spread for the EEPS-OEF method (Fig. 4, panel c) is large everywhere and non-localized (i.e. a basin-wide uniform value of approximately $2.5\,cm$). Additional amplitude in SSH spread for the EEPS-OEF occurs in the Aegean Sea, the Adriatic Sea and the Gulf of Gabes ($10°E$, $34°N$), as well as in the same regions identified for BHM-SVW-OEF but at smaller amplitude. For both methods, the average spread is relatively small (order $3\,cm$) and comparable to the SLA satellite errors (Dobricic et al., 2005).

Highest ensemble variance values are observed in both the BHM-SVW-OEF and EEPS-OEF responses at the location of the Algerian current anticyclonic eddies, one of which during

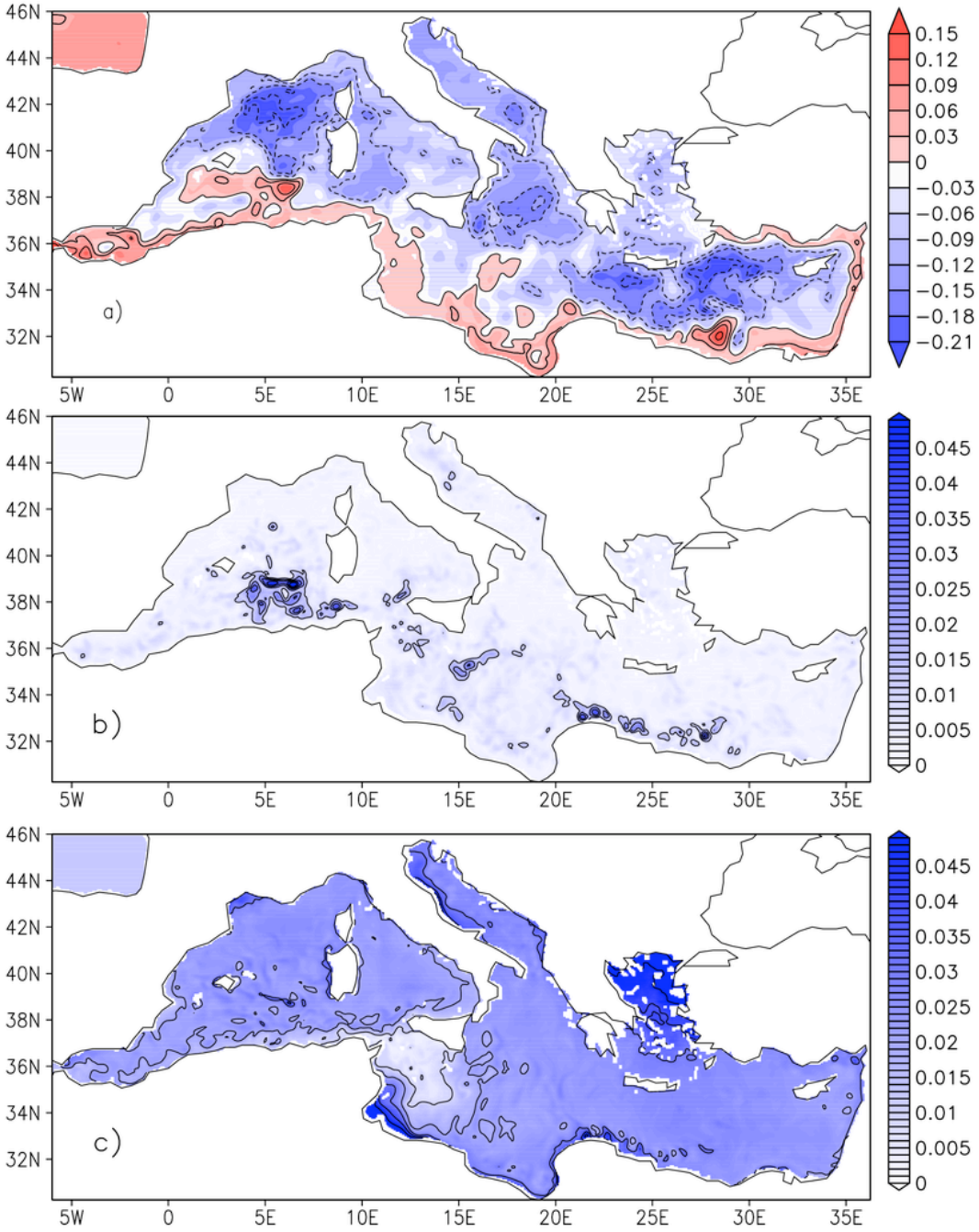

Figure 4: MFS1671 SSH fields for 17 February 2005, last day of forecast period (10F). a) Control forecast daily mean SSH, contour interval is 0.05 m. b) Standard Deviation [m] of SSH from BHM-SVW-OEF at 10F . c) Standard deviation [m] of SSH from EEPS-OEF at 10F. The contour interval in (b) and (c) is 0.01 m.

this period is centered at $6°E$, $-38.5°N$. Figure 5 shows how this structure is represented in the ensemble responses to both the BHM-SVW-OEF and EEPS-OEF. Figure 5 also depicts the effect of evolving currents in three ensemble members for each method on the simulated trajectories of 6 drifters released at the center of the anticyclone in each member at day 1F and tracked through day 10F. In this depiction, it is clear that the BHM-SVW-OEF members present a wider range of possible states than the EEPS-OEF members. A mesoscale eddy structure has detached in the period between 1F and 10F (not shown) from the northeastern edge of the anticyclone in BHM-SVW-OEF members 1 and 2, but not in member 3. The western border of the anticyclone is interacting with a second smaller eddy in BHM-SVW-OEF members 1 and 3, but this process is almost absent in BHM-SVW-OEF member 2. The cyclonic circulation north of the anticyclone strengthens in member 2 and not in the others. Conversely, the 3 EEPS-OEF members do exhibit similar variability, being different only in the strengthening/weakening of the cyclonic synoptic eddy on the northern border of the anticyclone. The simple trajectory simulations allow us to visualize better the effect of the uncertainty on the dynamical evolution of the anticyclonic eddy due to the deterministic components of the particle trajectories since no random dispersion due to lagrangian sub-grid scales was considered. In this simplified framework we observe that the EEPPS-OEF does not allow for any of the particles to exit the anticyclonic eddy, while the BHM-SVW-OEF exhibits a greater spread, i.e. members 2 and 3 show several particles escaping the eddy center in different directions.

Fontanet et al. (2004) explained the dynamics of similar Algerian current anticyclonic eddies in terms of two-dimensional turbulence. In particular they show that the high current amplitude core of the eddy is characterized by shear stresses and strains that can cause large changes in the paths of drifters released along the currents at the eddy core. Our results show that the uncertainty in the winds can produce changes in the eddy field that in turn determine large sensitivity in the particle trajectories due to such eddy field.

The BHM-SVW-OEF method seems to be more effective than EEPS-OEF in generating changes in the jets around the anticyclone and the interaction of the anticyclone with nearby mesoscale eddies. The pinch-off of the border of an anticyclone, the merging of two eddies and the cyclogenesis near an anticyclone are all familiar processes associated with nonlinear barotropic/baroclinic instabilities of open-ocean eddies (e.g. Pinardi and Robinson, 1987, McWilliams et al., 1983). The BHM-SVW-OEF method seems to be capable of amplifying,

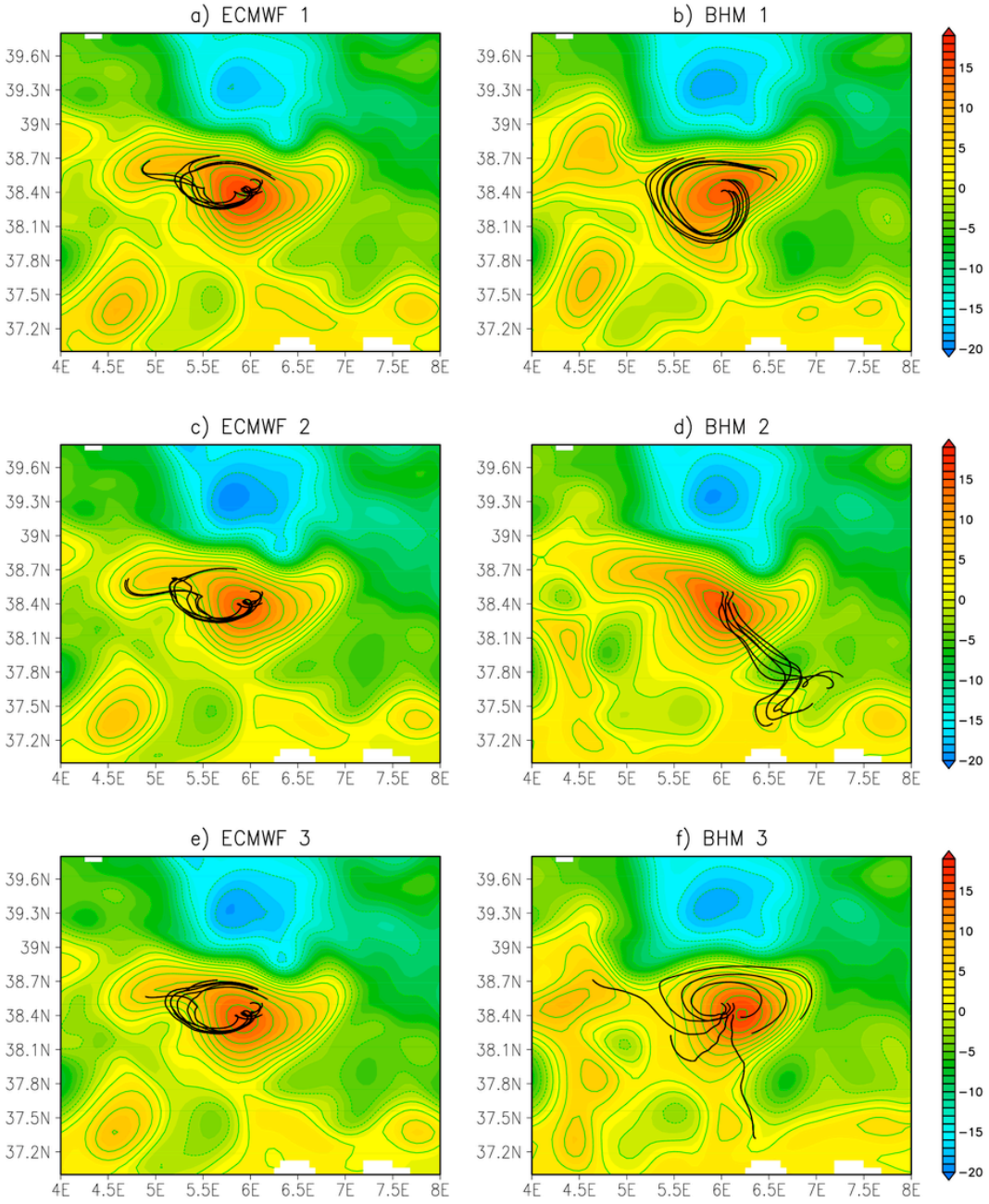

Figure 5: MFS1671 SSH mean daily fields at day 10F (17 February 2005) and 6 simulated particle trajectories (black lines) for EEPS-OEF members 1 to 3 (panels a, b and c), and for BHM-SVW-OEF members 1 to 3 (panels b, d and e). The contour interval is 0.02 m. Trajectories depict simulated drifter paths from 1F to 10F.

in one week, the initial condition perturbations at the time and space scales of the open-ocean baroclinic/barotropic instability processes.

As additional support for this interpretation, we show a density section across the Algerian current and the Gulf of Lyon gyre, where maximum spread is found at day 10F (Figure 6). Atlantic water, depicted as the lightest waters from the surface to 200 meters on the left side of the section (dark blues), flows along the Algerian coast over the salty and dense Mediterranean waters (reds). The region between $41°-42°N$ is the deep water formation area of the Gulf of Lyon gyre. A deep water formation event has already occurred (not shown) and dense water chimney remnants are still visible up to $100\,m$ depth. High values of BHM-SVW-OEF spread are found down to $400\,m$ (Fig. 6, panel b) consistent with the variability of the Algerian current anticyclonic eddy discussed above. The BHM-SVW-OEF method modified the eddy pycnocline and enables multiple realizations of baroclinic/barotropic instability processes. On the other hand, panel c shows that the EEPS-OEF also modifies the pycnocline but at different locations and at smaller amplitudes. EEPS-OEF does not perturb the pycnocline of the anticyclonic eddy, only the surface density of the cyclonic eddy north of it (see Figure 5), and it alters the pycnocline structure of the Algerian current.

We argue that the different ocean ensemble spread vertical structure is directly related to the different scales of the SVW fields. In the BHM-SVW-OEF case the spread is amplified around the unstable eddy jets, enabling multiple realizations of a process of barotropic/baroclinic instability, while in the EEPS-OEF case the spread is at lower amplitude and suggestive of large-scale, surface-intensified modes.

4.2 Low-Resolution Model Ensemble Response

In this section we study the response of the lower resolution forecasting model, MFS471, to the BHM-SVW-OEF and EEPS-OEF wind ensemble spread for the canonical ensemble experiment. We expect that the BHM-SVW-OEF method will be sensitive to the model resolution since the method amplifies the unstable modes associated with the ocean mesoscales and the MFS471 model is not eddy resolving (the Rossby radius of deformation is $10-15\,km$ in the Mediterranean Sea). The MFS471 is started from the upscaled initial condition at 1A, so the impact of low resolution is present throughout the analysis and forecast periods.

Figure 7 shows the effects of the lower resolution model in the control forecast SSH (top panel) which is smoother than the equivalent field of Figure 4. In the BHM-SVW-OEF

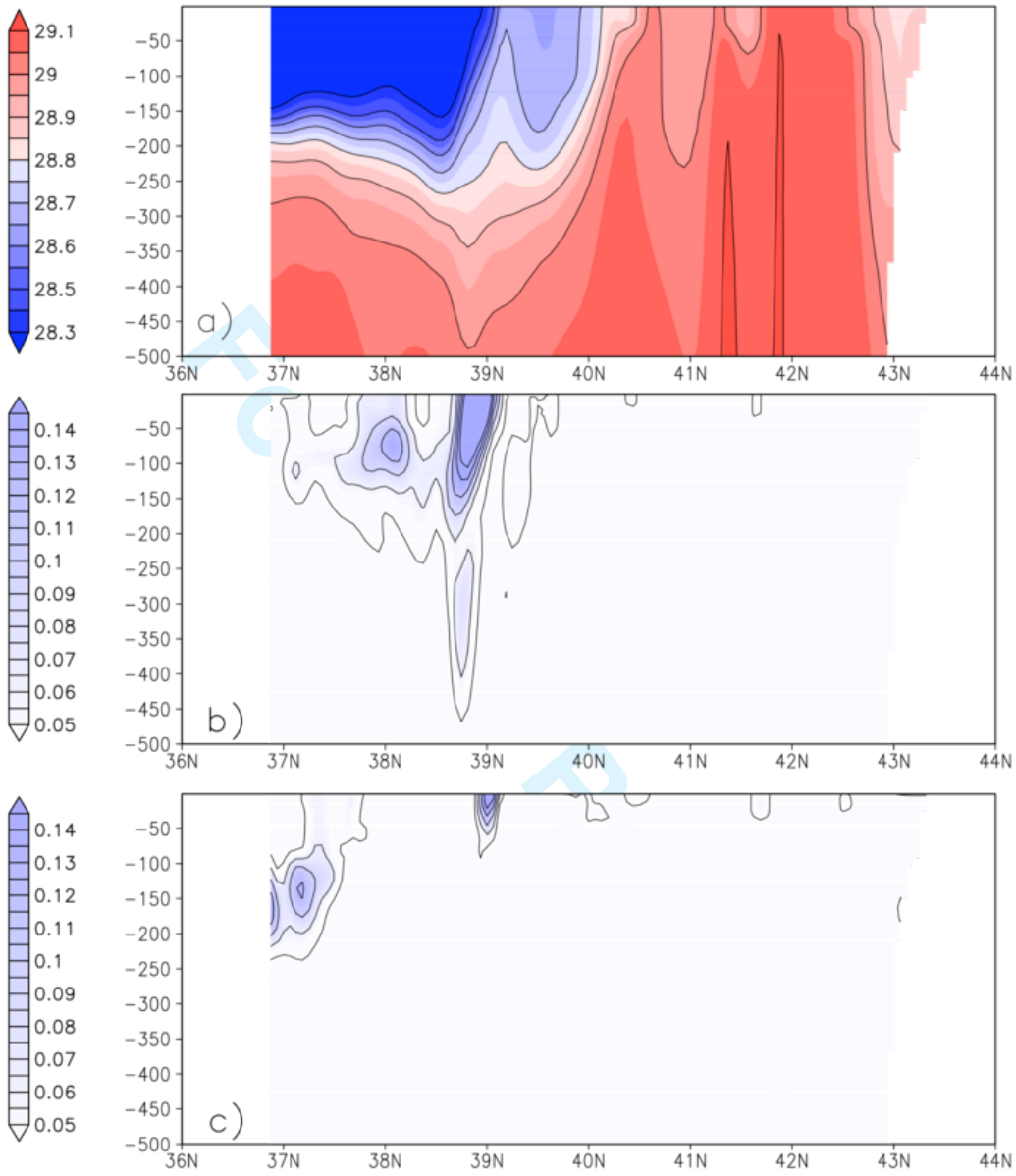

Figure 6: Meridional section of $\sigma = \rho - 1000$ $[kg\ m^{-3}]$ at $5°E$ (Algerian coast to the left, French coast to the right) for 17 February 2005 (10F). a) MFS1671 daily mean σ for the control forecast at 10F. The contour interval is $0.1\,kg\,m^{-3}$. b) σ standard deviation for BHM-SVW-OEF at 10F. c) σ standard deviation of EEPS-OEF at 10F. The contour interval in panels b and c is $0.03\,kg\,m^{-3}$.

spread (middle panel) the maxima are somewhat localized as in the high-resolution case, but the amplitudes are lower (below $1\,cm$ everywhere). The BHM-SVW-OEF method does not seem to be as effective at low resolution in amplifying the wind perturbations in the ocean response in the horizontal or vertical (not shown). On the other hand, the EEPS-OEF low-resolution experiment exhibits a similar response to the corresponding high-resolution case; both in terms of structures and amplitude. The localized spread areas (i.e. Algerian Current, Mersa Matruh gyre, etc.) are missing in the EEPS-OEF low-resolution case and the large-scale uniform response is dominant. The overall response is less sensitive to the model resolution than in the BHM-SVW-OEF case. This result supports the notion that the new method, BHM-SVW-OEF, amplifies the uncertainty due to winds at the ocean mesoscales, while EEPS-OEF is mainly changing the uniform, large-scale SSH patterns.

5 Comparison with an Initial Condition Perturbation Method

In this section we compare the wind ensemble perturbation methods above with a more traditional initial condition perturbation method. Pinardi et al. (2008) have developed a Thermocline Intensified Random Perturbation Ocean Ensemble Forecast method (TIRP-OEF) that prescribes initial perturbations with an *ad hoc* horizontal and vertical structure.

The temperature and salinity perturbed initial conditions, T_p and S_p, are written as:

$$T_p(x,y,z,t_0) = T(x,y,z,t_0) + p(x,y)\sum_{j=1}^{M} e_j f_j(z) \quad (2)$$

$$S_p(x,y,z,t_0) = S(x,y,z,t_0) + p(x,y)\sum_{j=1}^{M} e_j g_j(z) \quad (3)$$

where t_0 is the initial time, T and S are the temperature and salinity fields at 14A, $p(x,y)$ is a two-dimensional horizontal structure field with random amplitude, $f_j(z)$ and $g_j(z)$ are pre-defined vertical structure functions with amplitudes e_j. This method was originally used to generate Kalman filter background error ensembles in Evensen et al. (2003) and extended by Pinardi et al.(2008) with vertical structure functions.

For this experiment, 20 vertical structure functions were selected from a set of Empirical Orthogonal Functions (EOFs) computed from the analysis of the variance of a long ocean

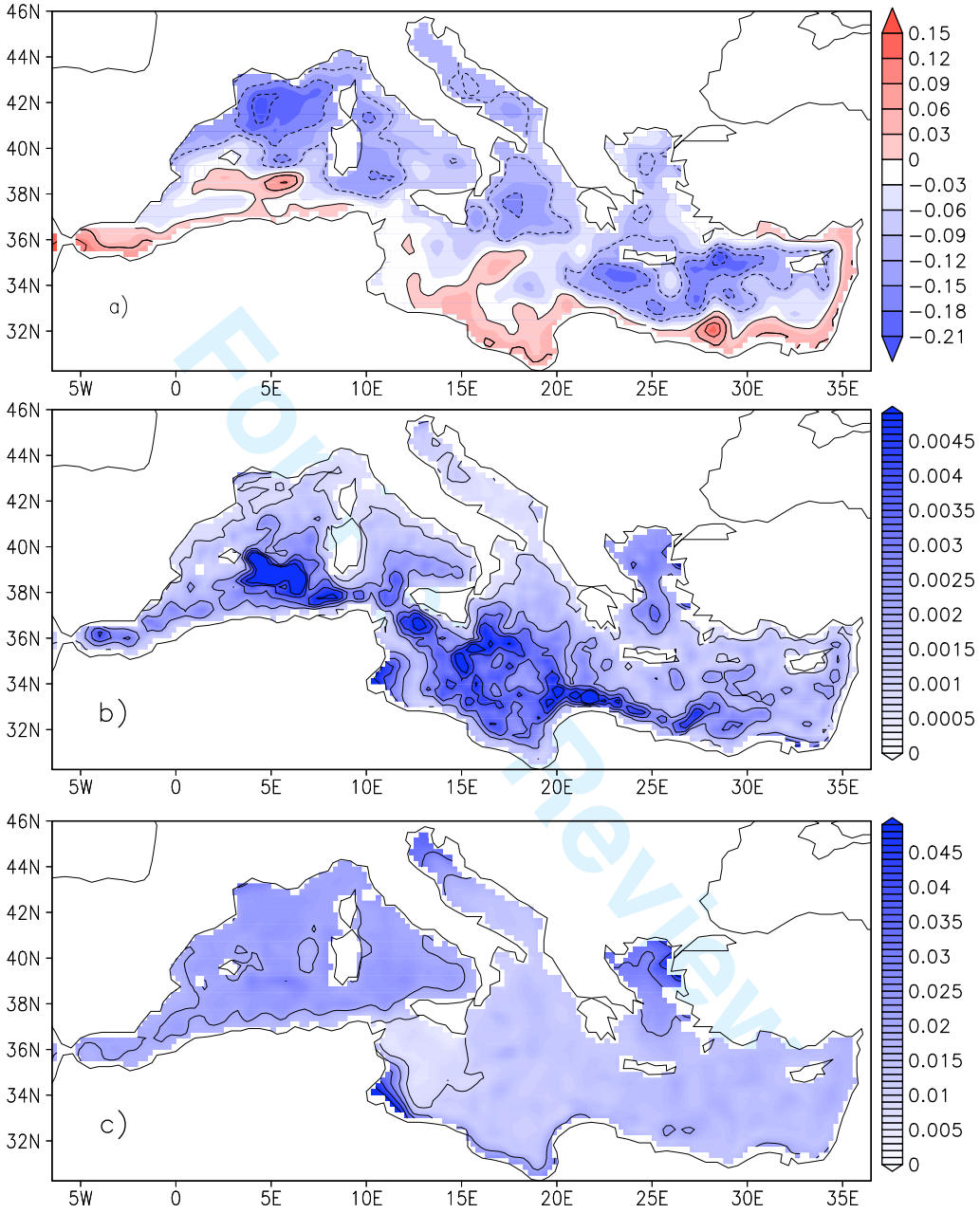

Figure 7: MFS471 SSH fields for 17 February 2005, last forecast day (10F). a) Daily mean SSH fields from the control forecast, contour interval is 0.05 m. b) Standard Deviation [m] of SSH for BHM-SVW-OEF. c) Standard deviation [m] of SSH for EEPS-OEF . The contour interval in panel (b) is 0.001 m; and in panel (c) is 0.01 m.

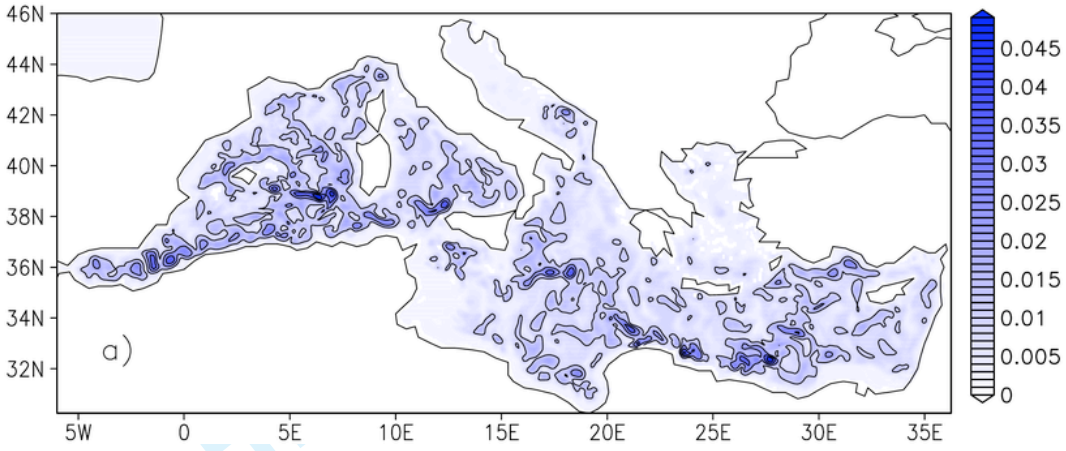

Figure 8: TIRP-OEF SSH standard deviation $[m]$ at 10F. The contour interval is $0.01\,m$.

model simulation. The e_j are the explained variance or eigenvalues for each mode. The EOFs have maximum amplitude at the depth of the thermocline, around $100 - 200\,m$, and they are discussed in Pinardi et al. (2008), Dobricic et al. (2005) and Sparnocchia et al. (2003). The p field at each grid point is modeled by a Gaussian function with a decay radius of $60\,km$ that roughly mimics the size of large mesoscale eddies in the Mediterranean Sea. The amplitude of p was set in order to obtain the horizontally integrated perturbations up to a value of $\pm 0.2\,cm$ in the SSH initial states. Initial perturbations of greater amplitude generate a noise signal in the forecast ensemble spread that does not allow clear identification of dynamical patterns in the forecast response (not shown).

The TIRP perturbations are clearly not consistent with data assimilation since each point in the domain has the same probability to be perturbed, regardless of whether or not an observation has been assimilated close by. Furthermore it is a method not strictly related to the wind-driven response and is *ad hoc* in that all free parameters (i.e. the number and type of EOFs, the horizontal structure radius and the amplitude) are decided on the basis of experience.

The TIRP-OEF method implemented here produces 10 perturbed initial T and S fields for the MFS1671 model. The initial condition ensemble members are forced by the single deterministic ECMWF wind forecast from 8 to 17 February 2005.

In Figure 8 we show the TIRP-OEF spread at 10F. The values are relatively large, up to $6\,cm$, and they are preferentially organized around mesoscale circulation structures. Three

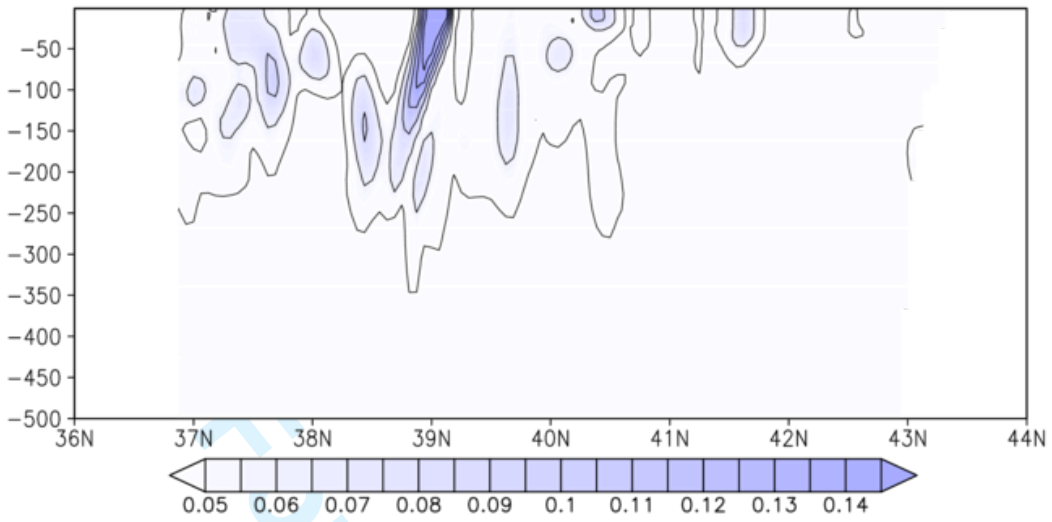

Figure 9: σ ($\sigma = \rho - 1000\,[kg\,m^{-3}]$) field standard deviation of TIRP-OEF at 10F. The contour interval is $0.1\,kg\,m^{-3}$.

maxima of SSH spread can be identified in the Algerian current, in the Ionian Sea and in the Levantine basin around the Mersa Matruh gyre, as in the case of BHM-SVW-OEF. The section at $5°E$ (Figure 9) reveals a structure of the density spread that is similar to what was observed in the BHM-SVW-OEF experiment (Fig. 6b), but at slightly smaller amplitude and shallower depths. The BHM-SVW-OEF and TIRP-OEF methods seem to have commensurate forecast ocean responses; more so than for BHM-SVW-OEF and EEPS-OEF. This suggests that the two ensemble methods activate similar dynamical processes.

We argued above that the BHM-SVW spread is associated with the ocean mixed barotropic-baroclinic instability processes. The TIRP perturbations are designed to produce modifications of the initial vertical stratification, thus changing the potential energy of the initial field at the thermocline, and potentially activating baroclinic/barotropic instabilities. Comparing Figures 4, 6, 8 and 9, it is evident that both methods can produce spread growing around either localized circulation structures, such as the Mersa-Matruh gyre and the Ionian Stream, or the mesoscale open ocean eddy fields, such as the anticyclonic eddy of the Algerian current. The TIRP-OEF spread however depends on the choices of the initial vertical EOFs (not shown) and the initial random amplitude. It will be difficult to generalize TIRP-OEF even in the Mediterranean Sea, where the thermocline depth changes are seasonal and the field is dominated by mesoscale eddies.

6 Ensemble Variance *versus* Forecast and Model Errors

A set of 47 BHM-SVW-OEF experiments of the same kind as described in the previous sections were performed for the period January-December 2006. Ensemble forecasts are produced once a week and there is no propagation of ensemble uncertainties between successive OEF cycles. Each cycle is considered to be independent even if the OEF initial conditions at day 1A are only 1 week apart and they are all coming from the sequential analysis cycle of MFS. The nearly one-year long experiment allows us to check the properties of the BHM-SVW-OEF spread for a period of time that covers an entire cycle of formation and destruction of the thermocline. It also allows us to compare this spread response with the forecast and model error variance.

In a perfect model scenario, wherein it is assumed that the model numerical integration does not introduce any error, the variance associated with the ensemble members around their ensemble mean is an optimal estimate of the forecast error. If M is the number of OEF cycles, and each cycle composed of N members, then Leutbecher and Palmer (2008) demonstrate that under the perfect model assumption the following limit is satisfied:

$$\lim_{M\to\infty} \frac{1}{M}\sum_{m=1}^{M} \gamma = 0 \quad and \quad \gamma = 1 - \frac{(N+1)\sigma_m^2}{(N-1)\epsilon_m^2} \tag{4}$$

where $\sigma_m^2 = \langle (X^m - \overline{X}^m)^2 \rangle$ is the variance of the m-th OEF cycle, X is in our case the temperature or salinity field at different depths and ϵ_m^2 is the mean square error of the m-th ensemble, computed as the difference between the ensemble mean and the truth, considered here to be the XBT and Argo observations. In our specific case we also compute the average of ϵ_m^2 and σ_m^2 between 1F and 10F.

In real applications the limit of γ usually differs from zero. Negative values of γ indicate over-dispersive ensemble behavior, i.e. the ensemble forecast variance is larger than mean squared forecast error. Positive values of γ indicate under-dispersive ensembles, i.e. ensemble variance too small compared to the mean squared error. For instance, Powell et al. (2008) show that the Intra American Seas ocean ensemble prediction system had values of $\gamma = -0.32$ and $\gamma = 0.88$ for SSH and SST respectively. The over-dispersive behavior of SSH in Powell et al. (2008) was artificially induced by inertia-gravity waves generated by the unbalanced initial conditions. Under-dispersive ensembles are usually more common than over-dispersive ensembles (Houtekamer and Mitchell, 2001) .

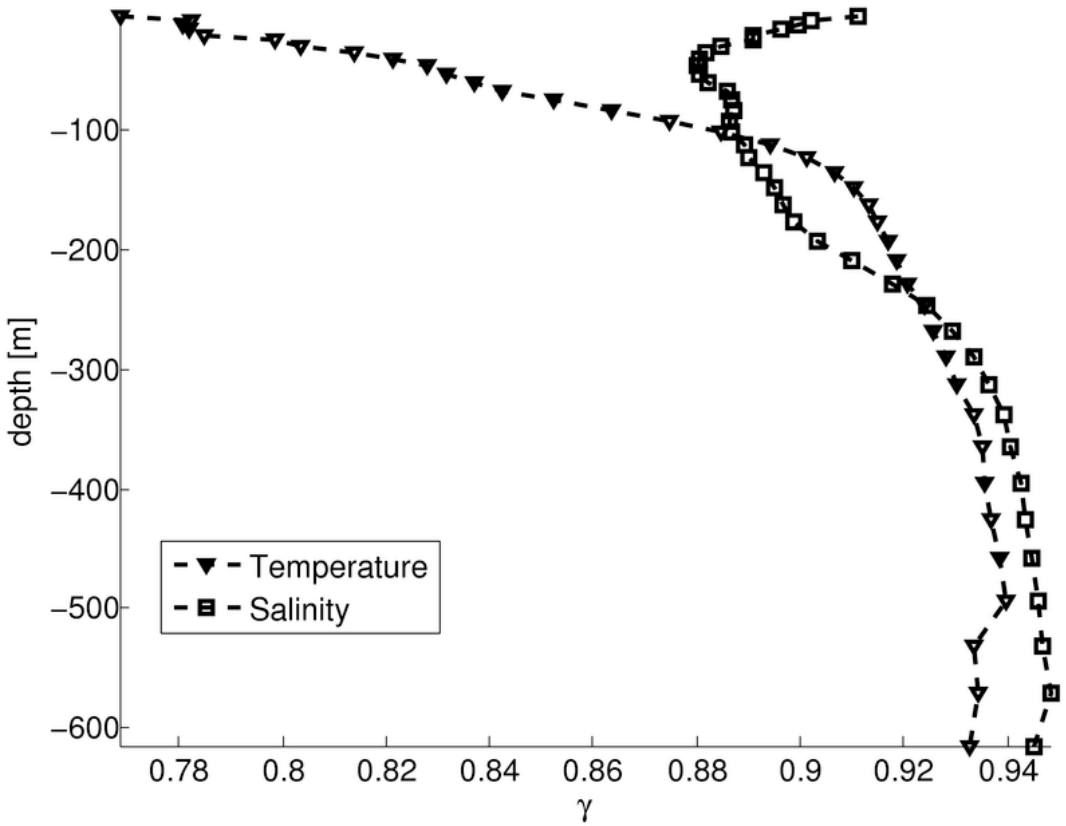

Figure 10: Values of γ (see text) as a function of depth and for temperature and salinity fields for the period January 2006-December 2006 and averaging between day 1F and 10F values.

The BHM-SVW-OEF is always under-dispersive, as shown in Figure 10. Over a series of 47 ensemble prediction cycles we found values of $\gamma = 0.89$ for SSH (not shown), while values for temperature and salinity range between 0.7 and 0.95. Under-dispersive minimum values are found in Figure 10 between 0 and $100\,m$ for temperature and between 30 and $200\,m$ for salinity. This result quantifies what was found before for the January-February 2005 study case. The BHM-SVW-OEF method amplifies the ensemble spread in the surface layer $(0 - 100\,m)$ and in the main thermocline $(100 - 200\,m)$, but is not efficient in exciting all forms of uncertainties that contribute to the total forecast error. In fact, the BHM-SVW-OEF method maps only the forecast uncertainties that project on the possible errors in the wind fields over the 14-day analysis cycle and it is reasonable that it will underestimate the total forecast error.

Another estimate of the forecast system error is given by the root mean square (rms) of the difference between the model simulation during analysis time and the observations; i.e. the so-called misfit (Dobricic et al., 2007). The rms of the misfits quantifies the errors due to data scarcity, data assimilation inadequacies and the limited representation of processes by the numerical model. The rms of the misfit is typically used as the estimate of the background field or first guess errors. We compare the vertical BHM-SVW-OEF ensemble spread to the rms of the misfit to show how much of the background error field the BHM-SVW-OEF method captures in different seasons.

Figure 11 shows that summer intensification of the rms misfit is reproduced by the BHM-SVW-OEF method but the amplitude is largely underestimated (i.e. note changing gray scales in Fig. 11). This large underestimation is partially due to the data scarcity in the computation of the misfits when compared to the ensemble spread computed over every grid point in the discretized Mediterranean domain. However, the BHM-SVW-OEF method is capable of producing, without any *ad hoc* assumptions, the seasonal errors due to the formation of the thermocline which is the most significant error in ocean forecasting models, associated with the forcing inaccuracies and the mesoscale eddy field. These results indicate that the BHM-SVW-OEF method could be used in the future to produce ensemble members that can quantify the model background error covariance matrix.

7 Conclusions

In this paper we have studied different methods of ocean ensemble forecasting applied to the Mediterranean Sea. We have developed a new method, called BHM-SVW-OEF, that uses the posterior realizations of winds coming from BHM-SVW distributions described in Part I of our work (Milliff et al., 2009). The method produces initial condition perturbations during a 14-day analysis cycle leading up to the 10-day forecast period, by forcing with the BHM-SVW realizations. Part I of this paper shows that initial condition spread in SSH and SST localize in high shear and eddy rich regions during the analysis cycle. Continuing with the BHM-SVW realizations in the forecast period, perturbations grow; doubling in amplitude in ten days. The BHM-SVW-OEF method generates an ocean forecast spread that concentrates in the ocean mesoscale eddy field. The variance at this scale is probably connected to mixed barotropic/baroclinic instabilities of the open ocean flow field.

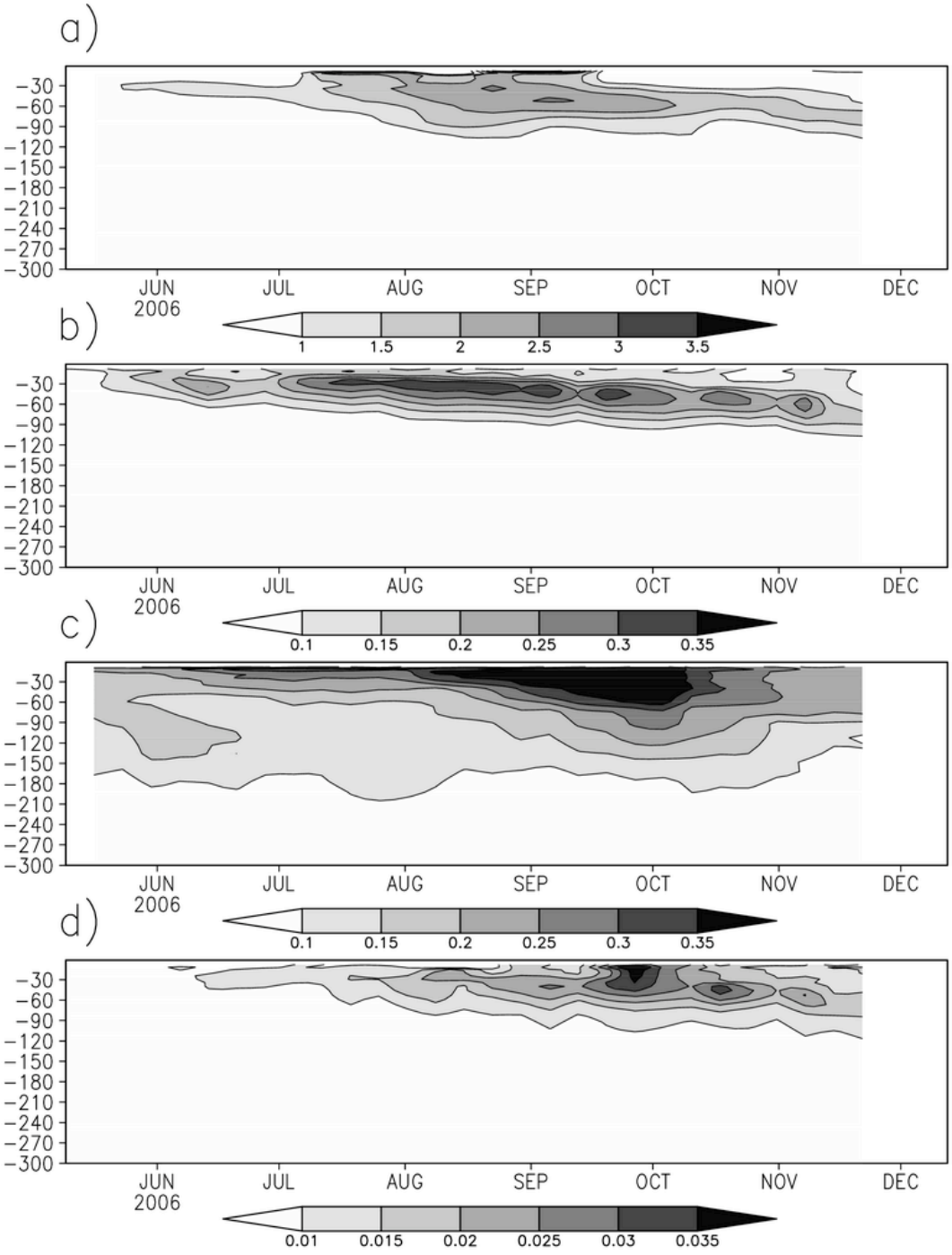

Figure 11: Vertical distribution of temperature and salinity root mean square of misfits and BHM-SVW-OEF ensemble spread averaged for the whole Mediterranean Sea for the period June-December 2006. a) Root mean square of misfit and b) BHM-SVW-OEF spread for temperature in $°C$. c) Root mean square of misfit and d) BHM-SVW-OEF spread for salinity in PSU.

The new method has been compared with two more traditional methods of generating ocean ensemble perturbations and forecasts. The first uses the ECMWF EPS surface winds starting from a single initial condition and forcing the ocean forecast ensemble with 10 realizations. The second is an *ad hoc* perturbation method for the T and S initial condition fields, i.e. the so-called Thermocline Intensified Random Perturbation or TIRP.

BHM and EEPS winds differ substantially during the forecast time. EEPS wind ensemble spread mimics the forecast error growth in the ten-day forecast period while BHM-SVW ensemble spread is constant over the same period. This is probably a short-coming of the BHM-SVW assumptions that can be readily improved in future versions. On the contrary, during the analysis period, the BHM-SVW distributions carefully track sources of surface wind forcing uncertainty. This uncertainty can be quantified in an objective way (Chin et al. 1999, Milliff et al. 1999, 2004) using abundant scatterometer and analysis data so as to yield realistic estimates of the wind uncertainties. EEPS winds instead try to maximize uncertainty in the growth of errors for the atmospheric forecast focused on middle troposphere geopotential height dynamics. The EEPS-SVW realizations exhibit large-scale differences in the surface winds (associated with synoptic disturbances of several hundred kilometers scale), while the BHM-SVW differ at finer scales (see Figure 3). Our results show that the finer scale differences in the BHM-SVW realizations can amplify the perturbations at the ocean eddy scales much more efficiently than the EEPS-SVW realizations.

Furthermore, the EEPS-SVW fields are not able to alter sufficiently the vertical stratification of the water column while the BHM-SVW-OEF vertical density spread peaks at the pycnocline of the eddies and retains significant amplitudes below. The BHM-SVW-OEF method activates a vertical, thermocline density ensemble spread that is much larger and eddy intensified than the one generated by the EEPS-OEF method. EEPS winds have been successfully applied to probabilistic modeling of ocean waves (Roulston, 2005) where depth-intensified response is less important. Our results suggest that short-term ocean circulation forecasts show a limited response to EEPS SVW realizations, mainly confined to the surface and at basin scales.

The experiments conducted with high- and low-resolution ocean models and the BHM and EEPS SVW realizations show a very different forecast response for the two methods. While the EEPS-OEF method yields almost identical ensemble spread between high- and low-resolution experiments, the BHM-SVW-OEF spread amplitude and structure depend

crucially on the high-resolution model eddy field representation. As such, the BHM-SVW-OEF method will be particularly useful for coastal ocean forecasting systems where the uncertainty due to winds is very important and high resolution is mandatory.

The comparison between BHM-SVW-OEF and TIRP-OEF methods demonstrates analogous responses in the ensemble spread generated by the two methods. The TIRP-OEF and the BHM-SVW-OEF produce thermocline intensified responses at the ocean mesoscales, with the former slightly more effective in the horizontal, and equivalent to the latter for the vertical ensemble spread. However, the TIRP method is not connected to data assimilation constraints, and is sensitive to the EOF modes chosen. The TIRP-OEF method is *ad hoc* and needs to be customized, probably at the seasonal and interannual time scales, for general applications.

Ensemble techniques are generally evaluated in terms of their ability to reduce and account for forecast error. We have shown that the BHM-SVW-OEF method does not fully represent the forecast or background field errors. In fact only a small *per centage* of the forecast error is accounted for in terms of ocean BHM-SVW-OEF spread. However, the vertical structure of the ensemble density spread mimics well the background field errors, being peaked at the thermocline and seasonally varying in depth (Fig. 11).

At this research stage of development we argue that the BHM-SVW-OEF offers a competitive method of producing short-term ocean ensemble forecasts if compared with other, more conventional, methods. Furthermore, it starts from an objective evaluation of uncertainty in the atmospheric forcing for the ocean models and it avoids discontinuities in variance between analysis and forecast periods. To our knowledge, it is the only method that insures continuity between the two periods, avoiding the excitement of large-scale gravity wave mode disturbances due to artificial changes in the surface wind. A natural extension of this work will be the consideration in the BHM-SVW of time varying wind variance errors for the forecast period and the combination of *ad hoc* TIRP perturbations with BHM-SVW during the analysis period.

Acknowledgments

The primary source of support for this work is the Physical Oceanography Program (Code 322) of the U.S. Office of Naval Research (ONR), Dr. Manuel Fiadeiro, Program Manager. Additional funding has been provided by ONR-Global to support scientific visits for Nadia Pinardi, and by the University of Bologna, Doctorate Program in Geophysics, and by the Istituto Nazionale di Geofisica e Vulcanologia, in support of Alessandro Bonazzi. The computing resources were kindly offered by the Istituto Nazionale di Geofisica e Vulcanologia, Sezione di Bologna, Gruppo Nazionale di Oceanografia Operativa.

REFERENCES

Auclair, F., P. Marsaleix and P. De Mey, Space-time structure and dynamics of the forecast error in a coastal circulation model of the Gulf of Lions. Dyn. Atmos. Oceans, 36, (2003) 309-346.

Brankart, J.M. and Pinardi, N. Abrupt cooling of the Mediterranean Levantine Intermediate Water at the beginning of the eighties: observational evidence and model simulation. Journal of Physical Oceanography 31 (8), (2001), 23072320.

Buizza, R. The ECMWF Ensemble Prediction System. In Predictability of Weather Climate, T. Palmer and R. Hagedorn, Eds. Cambridge University Press, 2006.

Buizza, R., and Palmer, T. N. The singular-vector structure of the atmospheric general circulation. Journal of Atmopheric Sciences 52, 9 (1995), 14341456.

Buongiorno-Nardelli, B., Larnicol, G., DAcunzo, G., Santoleri, R., Marullo, S., and LeTraon, P.-Y. Near Real Time SLA and SST products during 2-years of MFS pilot pro ject: processing, analysis of the variability and of the coupled patterns. Annales Geophysicae 21 (2003), 103 121.

Burillo, I. A-, G. Caniaux, M. Gavart, P. De Mey and R. Baraille. Assessing ocean-model sensitivity to wind forcing uncertainties. Geophys. Res. Letters, 29(18), (2002), 5.1-5.4.

Chin, T. M., Milliff, R. F., and Large, W. G. Basin-scale, high wavenumber sea surface wind elds from a multiresolution analysis of scat- terometer data. Journal of Atmospheric and Ocean Technology 15 (1998), 741763.

Dobricic, S., Pinardi, N., Adani, M., Bonazzi, A., Fratianni, C., and M. Tonani. Mediterranean Forecasting System: a new assimilation scheme for Sea Level Anomaly and its validation. Q. J. R. Meteorol. Soc. 131 (2005), 36273642.

Dobricic, S., Pinardi, N., Adani, M., Tonani, M., Fratianni, C., Bonazzi, A., and Fernandez, V. Daily oceanographic analyses by Mediterranean Forecasting System at basin scale. Ocean Sciences 3 (2007), 149157.

Evensen, G. The Ensemble Kalman Filter: theoretical formulation and practical implementation. Ocean Dynamics 53 (2003), 343367.

Farrell, B. F. Small error dynamics and the predictability of atmospheric ow. Journal of Atmopheric Sciences 47 (1990), 21912199.

Houtekamer, P.L. and Mitchell, H.L., A sequential ensemble Kalman filter for atmospheric data assimilation. Monthly Weather Review, 129, (2001) 123-137.

Korres G., Pinardi N. and Lascaratos A.The ocean response to low frequency interannual atmospheric variability in the Mediterranean Sea, Part I: Sensitivity experiments and energy analysis. Journal of Climate 13, (200) 705731.

Le Traon, P. Y., Nadal, F., and Ducet, N: An improved mapping method of multisatellite altimeter data, J. Atmos. Oceanic Tech- nol., 15, (2003) 522533.

Lacarra, J., and Talagrand, O. Short-range evolution of small perturbations in a barotropic model. Tellus 40A (1988), 8195.

Leutbecher, M., and Palmer, T. N. Ensemble forecasting. Journal of Computational Physics 227, 3 (2008), 515539.

Lucas M., N. Ayoub, T. Penduff, B. Barnier and P. De Mey. Stochastic study of the temperature response of the upper ocean to uncertainties in the atmospheric forcing in an Atlantic OGCM. Ocean Modelling 20, (2008), 90-113, 10.1016/j.ocemod.2007.07.006.

G. M. R. Manzella, F. Reseghetti, G. Coppini, M. Borghini, A. Cruzado, C. Galli, I. Gertman, T. Gervais, D. Hayes, C. Millot, A. Murashkovsky, E. zsoy, C. Tziavos, Z. Velasquez, and G. Zodiatis. The improvements of the ships of opportunity program in MFS-TEP. Ocean Sci., 3, (2007) 245-258.

McWilliams, J.C., E.D. Brown, H.L. Bryden, C.C. Ebbesmeyer, B.A. Elliot, R.H. Heinmiller, B.L. Hua, K.D. Leaman, E.J. Lindstrom, J.R. Luyten, S.E. McDowell, W.B. Owens, H. Perkins, J.F. Price, L. Regier, S.C. Riser, H.T. Rossby, T.B. Sanford, C.Y. Shen, B.A. Taft, and J.C. Van Leer. The local dynamics of eddies in the western North Atlantic. In: *Eddies in Marine Science*, A.R. Robinson, ed., Springer-Verlag, Berlin Heidelberg (1983) 92-113.

Milliff, R. F., A. Bonazzi, C.K.Wikle, N.Pinardi and L.M.Berliner. Ocean Ensemble Forecasting, Part I: Mediterranean Winds from a Bayesian Hierarchical Model. Submitted (2009)

Milliff, R.F., W.G. Large, J. Morzel, G. Danabasoglu, and Chin, T.M., Ocean general circulation model sensitivity to forcing from scatterometer winds. J. Geophys. Res., 104(C5), (1999) 11337-11358.

Milliff, R.F., J. Morzel, D.B. Chelton, M.H. Freilich, Wind stress curl and wind stress divergence biases from rain effects on QSCAT surface wind retrievals. Journal Atmospheric and Oceanic Technology, 21, (2004) 1216-1231.

Pettenuzzo, D., W.G. Large, N.Pinardi. On the corrections of ERA-40 surface ux products consistent with the Mediterranean heat and water budgets and the connection between basin surface total heat ux and NAO. Submitted (2009)

Pinardi, N., Allen, I., Demirov, E., DeMey, P., Korres, G., Lascaratos, A., LeTraon, P.-Y., Maillard, C., Manzella, G., and Tziavos, C. The Mediterranean ocean Forecasting System: rst phase of implementation (1998-2001). Annales Geophysicae, 21 (2003), 4962.

Pinardi, N. et al. (60 authors). The Mediterranean Operational Oceanography Network, Submitted (2009)

Pinardi, N., Bonazzi, A., Scoccimarro, E., Dobricic, S., Navarra, A., Ghiselli, A., and Veronesi, P. Very large ensemble ocean forecasting experiment using the Grid computing infrastructure. Bull. American Met. Soc. 89, 6 (2008), 799804.

Pinardi, N., and Robinson, A. R. Quasigeostrophic energetics of open ocean regions. Dynamics of Atmosphere and Oceans 10, 3 (1986), 185221.

Poulain, P. M., Barbanti, R., Font, J., Cruzado, A., Millot, C., Gertman, I., Griffa, A., Molcard, A., Rupolo, V., Bras, S. L., and de-la Villeon, L. P. Medargo: a drifting proler program in the Mediterranean Sea. Ocean Sciences 3 (2007), 379395.

Powell, B. S., Moore, A. M., Arango, H. G., DiLorenzo, E., Milliff, R. F., and Leben, R. R. Near real time assimilation and prediction in the Intra-American Sea with Regional Ocean Modelling System. Dynamics of Atmosphere and Oceans in print (2008).

Royle, J. A., Berliner, L. M., Wikle, C. K., and Milliff, R. M. A hierarchical spatial model for constructing wind elds from scatterometer data in the Labrador Sea. Springer-Verlag, 1998, ch. Case studies in Bayesian Statistics, pp. 367382.

Sparnocchia S., Pinardi N., and Demirov E. Multivariate Empirical Orthogonal Function analysis of the upper thermocline structure of the Mediterranean Sea from observations and model simulations. Annales Geophysicae 21 (1), (2003), 167187.

Tonani, M., Pinardi, N., Dobricic, S., Pujol, I., and Fratianni, C. A high-resolution free-surface model for the mediterranean sea. Ocean Sciences 4 (2008), 114.

Tonani, M., N. Pinardi, C. Fratianni, J. Pistoia and S. Dobricic. Forecast and Analysis Assessment through Skill Scores in the Mediterranean Sea. Ocean Sci. Discuss., 4, 189-212, 2007 (2009)

Wikle, C. K., Milliff, R. F., Nychka, D., and Berliner, L. M. Spatio-temporal hierarchical bayesian modelling: Tropical ocean surface winds. Journal of American Statistical Association, 97 (2001), 382397.